



A model-based optimization strategy to achieve fast and robust freeze-drying cycles

Brecht Vanbillemont^{a,*}, Anna-Lena Greiner^a, Vanessa Ehrl^a, Tim Menzen^a, Wolfgang Friess^b, Andrea Hawe^a

^a Coriolis Pharma Research GmbH, Martinsried 82152, Germany

^b Department of Pharmacy, Pharmaceutical Technology and Biopharmaceutics, Ludwig Maximilian University, Munich 81377, Germany

ARTICLE INFO

Keywords:

Biopharmaceuticals
Lyophilization
Primary drying
Mechanistic modelling
Process optimization
Quality-by-Design

ABSTRACT

Freeze-drying is a time and cost-intensive process. The primary drying phase is the main target in a process optimization exercise. Biopharmaceuticals require an amorphous matrix for stabilization, which may collapse during primary drying if the critical temperature of the formulation is exceeded. The risk of product collapse should be minimized during a process optimization to accomplish a robust process, while achieving an economical process time. Mechanistic models facilitate the search for an optimal primary drying protocol. We propose a novel two-stage shelf temperature optimization approach to maximize sublimation during the primary drying phase, without risking product collapse. The approach includes experiments to obtain high-resolution variability data of process parameters such as the heat transfer coefficient, vial dimensions and dried layer resistance. These process parameters variability data are incorporated into an uncertainty analysis to estimate the risk of failure of the protocol. This optimization approach enables to identify primary drying protocols that are faster and more robust than a classical approach. The methodology was experimentally verified using two formulations which allow for either aggressive or conservative freeze-drying of biopharmaceuticals.

1. Introduction

Freeze-drying or lyophilization is a unit operation designed to gently dry (bio)-pharmaceuticals in a low-temperature environment with the intention to improve long-term stability (Nail et al., 2002). A lyophilization process is time and cost intensive. Thereby, the primary drying phase alone consumes up to 40% of the total resources (i.e., electricity, nitrogen, water) required for a fill-and-finish process of a lyophilized product (Gamiz et al., 2019). Reducing the duration of the primary drying phase is therefore the focus of a freeze-drying process optimization exercise, while still maintaining the intended product attributes such as residual moisture and cake appearance.

Biopharmaceuticals typically need an amorphous matrix to keep the active pharmaceutical ingredient stable in the dried state (Carpenter et al., 1997). Collapse can occur during lyophilization, if the dried matrix exceeds its specific critical temperature, which can be determined by differential scanning calorimetry (DSC) or freeze-drying microscopy (FDM) (Nail et al., 2002). A sublimation process can be accelerated by

increasing the product temperature. However, the temperature at the sublimation interface must be kept below the critical temperature to achieve a structurally intact and elegant dried cake. Moreover, there are several equipment features limiting a process optimization such as maximum cooling/heating rates, lower pressure limit, and a condenser duct limiting the maximum sublimation rate (Patel et al., 2010).

The temperature at the sublimation interface can only be manipulated indirectly in a pharmaceutical freeze-drying process. It is the result of a complex interplay between all process parameters (i.e., shelf temperature, chamber pressure, freezing conditions), freeze-dryer design, and several material attributes related to the drug product (i.e., primary packaging, fill volume, selection and concentration of formulation components, etc.). Various examples of mechanistic models of the primary drying phase describing this complex interplay of parameters have been developed (Tang and Pikal, 2004; Fissore and Pisano, 2015; Mortier et al., 2016). For an in-depth recommendation on freeze-drying model practices the reader is referred to the literature (Nail et al., 2017; Tchessalov et al., 2022).

* Corresponding author.

E-mail addresses: Brecht.Vanbillemont@Coriolis-Pharma.com (B. Vanbillemont), Tim.Menzen@Coriolis-Pharma.com (T. Menzen), Wolfgang.Friess@lrz.uni-muenchen.de (W. Friess), Andrea.Hawe@Coriolis-Pharma.com (A. Hawe).

<https://doi.org/10.1016/j.ijpx.2023.100180>

Received 5 December 2022; Received in revised form 22 March 2023; Accepted 8 April 2023

Available online 10 April 2023

2590-1567/© 2023 The Authors. Published by Elsevier B.V. This is an open access article under the CC BY-NC-ND license (<http://creativecommons.org/licenses/by-nc-nd/4.0/>).

The two key manipulative parameters of the primary drying phase are shelf temperature and chamber pressure. Mechanistic models can assist in the decision on the most optimal set points. A common methodology is to create a graphical design space that illustrates both the process limits and the interdependency of the manipulative parameters (Patel and Pikal, 2013; Carfagna et al., 2020). Such an approach assumes static process parameters. Yet, it is known that the physical state of the product continuously evolves during primary drying (Vanbillemont et al., 2020). On top of the frozen product, a dried product layer is formed through which the sublimed water molecules must pass on their way to the condenser. As primary drying progresses, this vapor flow will therefore encounter a growing resistance. This dried product layer resistance originates from Knudsen flow inside the tortuous micro-sized pores (Pikal et al., 1984).

A graphical design space is static as it assumes the highest resistance value associated with the maximal dried layer thickness, which is only valid at the end of primary drying. This is not an optimal way of approaching the primary drying phase. During the initial phase (i.e., first 20 to 30%) of primary drying, the resistance of the thin dried layer formed is still rather low. Thus, more aggressive, dynamic primary drying protocols can be applied in this early phase without provoking collapse (Mortier et al., 2016; De Meyer et al., 2017; Vanbillemont et al., 2020). However, dynamic protocols are hard to implement on most classic freeze-dryer controllers, due to software restrictions. Moreover, the dynamic approach is challenging from a process control and regulatory perspective since manipulative parameters will be varied across batches. Application of a two-stage shelf temperature protocol during primary drying could render the benefits of a dynamic protocol and is straightforward to program in a classic freeze-dryer controller. Like the dynamic protocols, a two-stage shelf temperature protocol can maximize the sublimation rate near the process limits during the entire progress of primary drying leading to a more economical process.

In addition, regulatory authorities require justification of the proposed freeze-drying process protocol to assure consistent product quality across the product development trajectory and post-approval lifecycle (Rhieu et al., 2020). Thermal analysis of the freeze-concentrate combined with the application of mechanistic models can provide the required scientific rationale for process design choices.

During an uncertainty analysis, various sources of variabilities are taken into consideration and their impact on the outcomes of the process are estimated. The risk of process failures, such as collapse originating from a specific freeze-drying protocol, can be estimated using uncertainty analysis methodology (Vanbillemont et al., 2020). Because lyophilization is an inherently variable process (i.e., stochastic nature of ice nucleation, edge vial effect, etc.) (Pisano et al., 2011; Leys et al., 2020; Strongrich and Alexeenko, 2021), uncertainty analysis of mechanistic models can strongly aid in the risk assessment of primary drying protocols.

The objective of our work was to develop and verify a process development methodology that can provide fast and at the same time robust primary drying protocols. Besides the verification we aimed to benchmark our novel approach against an established approach proposed by Tang & Pikal (Tang and Pikal, 2004). For this purpose, detailed mechanistic models were constructed. This yielded the opportunity for in-silico process simulation and for exploring a multitude of protocols to find the most economical one. A two-stage shelf temperature protocol was employed, which enabled further process optimization although at the cost of a higher protocol complexity. This additional complexity exemplifies the need for in-silico process optimization. Next, the variabilities associated with the lyophilization process of our model formulations were characterized with high resolution. These were essential to be able to estimate the risk of process failures, and thus robustness, of a given primary drying protocol.

2. Materials and methods

2.1. Materials

Highly purified lysozyme (Ovobest, Neuenkirchen-Vörden, Germany) was used as model protein. Two formulations with different critical temperature (T_c) were designed by adapting the protein concentration and concentration/type of lyoprotectant to challenge the process optimization approach under conservative and aggressive lyophilization conditions. The 'high' T_c formulation enabling aggressive freeze-drying conditions consisted of 2 mM histidine, 10 mg/ml lysozyme, 5% (w/v) 2-hydroxypropyl- β -cyclodextrin and 0.03% (w/v) polysorbate 80 at a pH of 6.5. The 'low' T_c formulation used for the conservative processes contained 2 mM histidine, 1 mg/ml lysozyme, 10% (w/v) sucrose and 0.03% (w/v) polysorbate 80 at a pH of 6.5. All excipients were of compendial quality. Ultra-purified grade water was applied (Millipore, Darmstadt, Germany). Lyophilization vials (6 mL, 6R Fiolax clear) were obtained from Schott (Mainz, Germany), and 20 mm bromobutyl 4023/50 Fluorotec lyophilization stoppers and flip-off caps were acquired from West Pharma (Exton, PA, USA).

2.2. Lyophilization

Lyophilization was performed in an Epsilon 2-12D freeze-dryer (four functional shelves with a total area of 0.63 m²) using LPC-32 control software from M. Christ (Osterode am Harz, Germany). All experiments were performed using one full shelf load containing 334 vials in a hexagonal loading pattern with a bottomless tray system on the second shelf from the bottom. All samples were semi-stoppered. The condenser is located directly under the shelf stack. Due to the absence of a restricting duct between drying chamber and condenser, a limitation by a choked flow condition was not considered in process design and modelling.

2.3. Critical temperature determination

The critical temperature (T_c) of both formulations under study was determined by use of a FDSC 196 freeze-drying microscope (Linkam, Surray, UK) with a 10-fold magnification. An aliquot of the formulation (2 μ l) was pipetted on a quartz crucible. A horseshoe-shaped spacer ring ensured a defined distance between quartz crucible and cover slip. The sample was frozen with a rate of 1 °C/min to -50 °C. After exhausting to a vacuum of 10 Pa, the sample was heated at 1 °C/min and pictures were acquired every 2 s. After the experiment, all images were inspected for signs of collapse.

2.4. Contact angle measurements

The contact angle between the glass vial and formulation was measured in triplicate using a DSA25E Drop Shape Analyzer (Krüss, Hamburg, Germany). A sessile drop test was performed on the outer surface of the vial. An ellipse tangent method was applied to estimate the contact angle at both sides of the droplet.

2.5. Residual moisture content

The residual moisture content of lyophilized samples was determined using a headspace coulometric Karl-Fischer titration method utilizing an Aqua 40.00 Vario (ECH, Halle, Germany). Five samples selected across the shelf, including edge and center vials, were characterized by heating 30 mg of the dried cake to 120 °C and titrating the resultant water in the headspace of the vial.

2.6. Mechanistic model of the primary drying phase

The mechanistic model of the primary drying phase of a pharmaceutical lyophilization process was constructed in Python v3.7.0 (Bea-

verton, OR, USA). The model is a heat-mass balance that consists of a set of mathematical equations (Eq. (1) till 4) that were solved simultaneously (Vanbillemont et al., 2020).

$$P_i = -\frac{-A_p \Delta H_{sub} P_c - A_v K_v R_p M(T_s - T_i - \Delta T)}{A_p \Delta H_{sub}} \quad (1)$$

$$P_i = A_{P_i} - \frac{B_{P_i}}{T_i} + C_{P_i} \ln(T_i) - D_{P_i} T_i \quad (2)$$

$$\Delta T = \frac{a \frac{(L_i - L_d)(P_i - P_c)}{R_p} - b(L_i - L_d)(T_i - T_s)}{1 - b(L_i - L_d)} \quad (3)$$

$$\Delta H_{sub} = A_{H_{sub}} + B_{H_{sub}} T_i - C_{H_{sub}} T_i^2 + D_{H_{sub}} e^{-\left(\frac{T_i}{E_{H_{sub}}}\right)^2} \quad (4)$$

This set of equations describes the relation between process parameters such as fluid temperature inside the shelves (T_s) and chamber pressure (P_c), the material attributes such as the dried product layer resistance (R_p), heat transfer coefficient (K_v), frozen fill height (L_v), area of the bottom of the vial (A_v) and the cross section of the cake (A_p), as well as the process outcomes sublimation interface temperature (T_i), dried layer height (L_d), and temperature differential across the frozen product (ΔT). Next, several coefficients and constants were applied. M represents the molecular weight of water; A_{P_i} to D_{P_i} are coefficients to describe the equilibrium of T_i and the partial vapor pressure (P_i) (Mortier et al., 2016); a and b are SI converted coefficients that describe heat conduction in the frozen product layer (Tang et al., 2006); $A_{H_{sub}}$ to $E_{H_{sub}}$ describe an empirical relationship between the latent heat of sublimation (ΔH_{sub}) and T_i (Murphy and Koop, 2005).

These equations physically represent a planar dried layer that gradually appears on top of a receding frozen product layer as the sublimation process progresses. Water vapor escaping the frozen layer is hindered by the growing dried layer. Moreover, the heat supplied by the freeze-dryer to the frozen product is solely used for sublimation (Velardi and Barresi, 2008; Patel and Pikal, 2013).

2.7. Experimental determination of variability terms for critical input parameters

An evaluation of the primary drying model (Eqs. (1 to 4)) was performed to determine which input parameters can be measured or estimated and could result in intra batch variability within the primary drying phase. Eight parameters, A_p , A_v , L_v , T_s , P_c , R_p , K_v and L_d were deemed to be critical. Specific experiments were setup to determine the variability terms for each of these critical input parameters.

2.7.1. Variability terms for container and equipment

Variability terms for the vial and product area (A_v and A_p) were determined by measuring the outer diameter (d_o) of 100 6R vials by using a stainless-steel caliper with a resolution of 0.01 mm. It is assumed that the vials have a cylindrical shape and that the average (\bar{d}_o) and standard deviation (σ_{d_o}) were sufficient as variability terms to describe the observed variation in A_v .

Manufacturer details for the vial wall thickness and its variation, t_w 1.0 mm and σ_{t_w} 0.1 mm, were applied to estimate the inner diameter (d_i) and its standard deviation (σ_{d_i}) using Eqs. (5 and 6). The average (\bar{d}_i) and standard deviation (σ_{d_i}) were used as variability terms to describe A_p .

$$d_i = d_o - 2 t_w \quad (5)$$

$$\sigma_{d_i} = \sqrt{\sigma_{d_o}^2 + \sigma_{t_w}^2} \quad (6)$$

Sixty vials were filled with 3.0 ml of either formulation, placed on center positions of the shelf and subsequently frozen to -45 °C. The height of the frozen product plug (L_i) was determined using the caliper.

Both average (\bar{L}_i) and standard deviation (σ_{L_i}) of L_i were used as variability terms. Normality of the distributions of d_o and L_i was examined by visually assessing the similarity of histograms with 10 bins of the observed and the expected datasets.

A spatial distribution of P_c and T_s across the shelf or chamber can be expected during the primary drying phase (Strongrich and Alexeenko, 2021; Rasetto et al., 2010). Moreover, due to the on-off control algorithms of the lyophilizer, also temporal variations of P_c and T_s will occur. The freeze-dryer annual service documentation reported maximal deviations of 1 Pa for P_c and 1 °C for T_s which are related to these spatio-temporal distributions.

2.7.2. Variability terms for the heat transfer

The heat transfer coefficient (K_v) and variability terms for the applied freeze-dryer and 6R vials combination were gravimetrically determined (Pisano et al., 2011). The heat transfer was characterized initially at 5, 10, 16, 20, and 25 Pa each with 100 vials filled with 3.0 ml water and spread across a full shelf load including center and edge positions. The vials were frozen to -30 °C followed by sublimation for 3 h at a T_s of -15 °C. Product temperature was observed with four compact PT100 (RTD) with a radius of 1.5 mm and four thermocouples type-K (TC) placed in vials which were not used for further analysis and evenly distributed across the shelf including edge and center sample positions. The K_v was estimated using Eq. (7) with m_{sub} representing the sublimated mass and T_b the bottom product temperature determined using the product sensors.

$$K_v = \frac{m_{sub} \Delta H_{sub}}{A_v M \int (T_s - T_b) dt} \quad (7)$$

The heat transfer values of the 100 vials over the 5 different pressure experiments were used for the K_v regression. At first, the shelf average heat transfer coefficient (\bar{K}_v) in function of P_c was described by determining coefficients α , β and γ using a weighted non-linear regression according to Eq. (8) with the inverse of the relative standard deviation (RSD) at each pressure level as the weights (Vanbillemont and De Beer, 2020). The RSD of K_v (RSD_{K_v}) was calculated for each pressure level and described using a linear regression according to Eq. (9) with coefficients a_{K_v} and b_{K_v} .

$$\bar{K}_v = \alpha + \frac{\beta P_c}{1 + \gamma P_c} \quad (8)$$

$$RSD_{K_v} = a_{K_v} + b_{K_v} P_c \quad (9)$$

Next, an empirical distribution was constructed by normalizing all K_v datapoints across all pressure levels by using the average (\bar{K}_v) and standard deviation (σ_{K_v}) value within a pressure level experiment (see Eq. (10)).

$$\hat{K}_v = \frac{K_v(P_c) - \bar{K}_v(P_c)}{\sigma_{K_v}(P_c)} \quad (10)$$

At last, an independent K_v verification experiment was run at a P_c of 22 Pa and T_s of -5 °C to evaluate the independence of the \bar{K}_v and RSD_{K_v} regressions from T_s .

2.7.3. Variability terms for the dried product layer resistance

The dried product layer resistance (R_p) and variability terms were determined for both formulations in independent lyophilization cycles. Fifty vials were filled with 3.0 ml of formulation and placed in the center location of the shelf. To preserve the hexagonal stacking pattern, the remaining shelf space was packed with empty vials. The eight most center positions (i.e., at least two vials away from an empty vial) were fitted with product temperature sensors ($4 \times$ RTD and $4 \times$ TC).

The freeze-drying protocol for the 'high' T_c formulation was freezing to T_s : -30 °C for 5 h with a cooling rate of 1 °C/min, primary drying at T_s : -5 °C and P_c 20 Pa and secondary drying at T_s : 25 °C and P_c : 20 Pa for 6 h with a heating rate of 0.25 °C/min. The protocol for the 'low' T_c

formulation was more conservative with freezing to T_s : -45 °C for 5 h with a cooling rate of 1 °C/min, primary drying at T_s : -30 °C and P_c : 10 Pa and secondary drying T_s : 25 °C and P_c : 10 Pa for 6 h with a heating rate of 0.25 °C/min. The primary drying time of these cycles was controlled using comparative pressure measurement.

The R_p profile of each temperature monitored product was calculated by fitting the mechanistic primary drying model (see section 2.6) to the product temperature trace (T_b) and employing the K_v^- regression. The dried layer height (L_d) was estimated using Eq. (11) with ρ denoting ice density and φ the estimated dried layer porosity. Drying progression was calculated as the fraction of L_d from L_t .

$$L_d = \frac{m_{sub}}{\rho \varphi A_p} \quad (11)$$

Negative R_p values and R_p values associated with vials that show an upwards trend of T_b at the end of primary drying (i.e., due to loss of ice contact) were omitted as not being representative. Please note that the RTD sensors lost full ice contact earlier than the TC sensors. An average R_p profile (\bar{R}_p) was regressed for each formulation from all R_p and associated L_d values according to Eq. (12) by determining the R_{p0} , A and B coefficients (Scutella et al., 2018).

$$\bar{R}_p = R_{p0} + \frac{A L_d}{1 + B L_d} \quad (12)$$

The drying progression was split into 33 equidistant bins containing the associated R_p values of all eight monitored vials. As variability term, the standard deviation (σ_{R_p}) was calculated by pooling the standard deviation of each of the 33 bins (Vanbillemont et al., 2020).

2.8. Uncertainty analysis of a freeze-drying protocol

For each suggested primary drying protocol (i.e., temporal combination of T_s and P_c), an uncertainty analysis was employed to verify that the protocol was within an acceptable risk of failure (RoF). A failure was defined as the sublimation interface temperature (T_i) being equal or exceeding the critical temperature (T_c) at any point during the protocol.

The uncertainty analysis was setup by applying the mechanistic primary drying model in a Monte Carlo approach with a temporal resolution of 60 s. A sample size of 2^{12} was chosen (i.e., 4096) to comply with Sobol sampling conditions (Sobol, 1967) and have a statistical meaningful data set. At each timepoint a parameter variability space with 4096 samples was constructed by combining distributions of each of the input parameters (i.e., A_p , A_v , L_t , T_s , P_c , R_p , K_v , and L_d). The variability space of A_p and A_v were constructed by random sampling from a normal distribution defined by \bar{d}_i and σ_{di} , or \bar{d}_o and σ_{do} respectively and calculating the area of a circle. The L_t variability space was also generated by random sampling from a normal distribution defined by \bar{L}_t and σ_{L_t} . For T_s and P_c , a quasi-uniform sampling approach (Sobol, 1967) was applied in the variability space defined by the freeze-drying protocol enlarged with a $T_s \pm 1$ °C and a $P_c \pm 1$ Pa. Next, the heat transfer coefficient variability space was constructed by random sampling from the empirical normalized distribution (see section 2.7.2.), followed by rescaling the normalized K_v values using the K_v^- and RSD_{K_v} obtained from their regressions (Eqs. (8 and 9)) using the P_c from the associated P_c variability space. For dried layer resistance, a variability space was constructed by randomly sampling from the normal distribution defined by \bar{R}_p and σ_{R_p} . At last, the variability space for the dried layer length (L_d) was constructed by error propagation. This was achieved by using the distribution of L_d obtained as a result of the last timepoint, as input for the next timepoint.

At each timepoint of the prediction, a new parameter variability space with size 8×4096 was constructed. This is necessary since L_d increases during the progress of primary drying and is due to the interdependency of various input parameters (see Eqs. (8, 9 and 12)). The primary drying model was applied on this dynamic parameter variability space and a distribution of model outputs (i.e., T_i and L_d) was

Table 1

Summary of the optimization factors and their intervals for both formulation within this study.

Optimization factor	'High' T_c Formulation		'Low' T_c Formulation	
	Low	High	Low	High
Stage 1 T_s [°C]	15	50	-33	-20
Stage 1 hold time [h]	0.2	2	0.5	20
T_s ramp [°C/h]	2	60	0.15	0.6
Stage 2 T_s [°C]	10	45	-33	-25
P_c [Pa]	5	25	5	25

Table 2

Overview of the constants and their values used in the optimization exercise.

Constant	Value	Unit	Source
M	0.018015	kg/mol	(Vanbillemont and De Beer, 2020)
A_{Pi}	9.550426	Pa	(Mortier et al., 2016)
B_{Pi}	5723.2658	K	(Mortier et al., 2016)
C_{Pi}	3.53068	1/K	(Mortier et al., 2016)
D_{Pi}	0.00728332	Pa	(Mortier et al., 2016)
a	889,200	-	(Tang et al., 2006)
b	1.02	-	(Tang et al., 2006)
A_{Hsub}	$4.68 \cdot 10^4$	J/mol	(Murphy and Koop, 2005)
B_{Hsub}	35.9	J/(mol K)	(Murphy and Koop, 2005)
C_{Hsub}	0.0741	J/(mol K ²)	(Murphy and Koop, 2005)
D_{Hsub}	542	J/mol	(Murphy and Koop, 2005)
E_{Hsub}	124	K ²	(Murphy and Koop, 2005)
ρ	919.4	kg/m ³	(Vanbillemont et al., 2020)
φ	0.939* / 0.898**	-	Formulation composition

*Represents a value used for the 'high' T_c formulation and ** for the 'low' T_c formulation.

achieved for the freeze-drying protocol with a similar temporal resolution of 60 s.

2.9. Process optimization strategy

A flexible two-stage shelf temperature regime was applied to maximize the sublimation rate by counteracting the increase in dried layer resistance over the progress of primary drying. At first, a fixed ramp at 1 °C/min towards a stage 1 T_s was programmed in the protocol. Next, the stage 1 T_s was maintained for a defined time followed by a T_s ramp at a defined rate towards a lower stage 2 T_s . At last, this stage 2 T_s was maintained until the end of primary drying prediction.

The optimization strategy consisted in creating an optimization space defined by the five factors that describes the flexible two-stage primary drying protocol. Table 1 gives an overview of these factors and their intervals for both formulations within this study. The intervals were based on experience with these formulations. Using a Sobol sampling approach (Sobol, 1967), 4096 combinations of these 5 factors were sampled quasi-uniform and resultant primary drying protocols constructed.

The optimal protocol for each of the formulations was identified by performing the uncertainty analysis of the primary drying model on all 4096 protocols. The criterion for success of a single protocol was defined by the outcomes of the uncertainty analysis. At first, for each timepoint within the prediction of a single protocol, the T_i distribution was used for evaluation of the failure criteria. In this study an RoF of 0.1% was deemed acceptable. Therefore, the 99.9% percentile of the T_i distribution at each timepoint of the protocol (i.e., p : 99.9% T_i) was determined and continuously compared with T_c . If the 99.9% percentile of the T_i distribution exceeded or was equal to T_c at any timepoint during a protocol evaluation, the simulation was aborted and this protocol was deemed unfit, i.e., a failure. Furthermore, the maximal p : 99.9% T_i across the entire protocol was also determined (i.e., $\max p$: 99.9% T_i).

In a next step, when a protocol was deemed robust (i.e., $\max p$: 99.9% $T_i < T_c$), the L_d output distribution at each timepoint was compared with

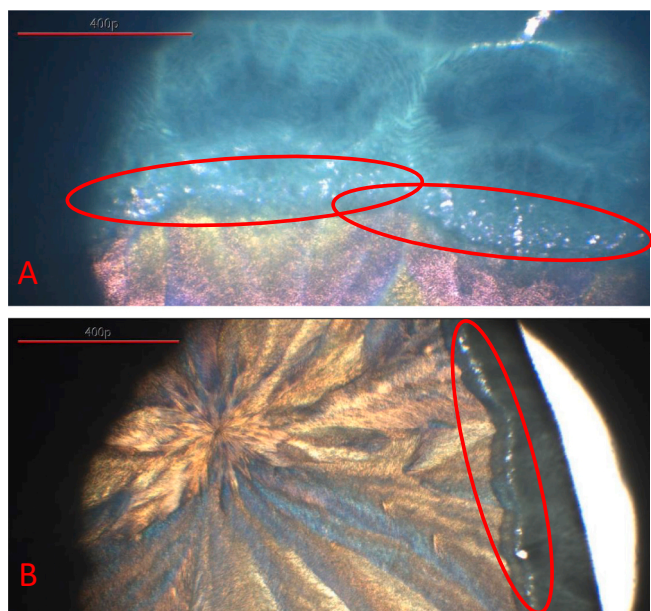


Fig. 1. Freeze-dry microscope images of the ‘High’ (A) and ‘Low’ (B) T_c formulations. Signs of collapse are indicated with red circles. The red line in the left top corner represents 400 px or 222 μm . (For interpretation of the references to colour in this figure legend, the reader is referred to the web version of this article.)

the associated L_t values from the parameter variability space to evaluate how many samples were free of ice (i.e., $L_d \geq L_t$). The process time when 99.9% of all samples were predicted to be free of ice was recorded as the primary drying time for that protocol.

In a last step, all robust protocols were ranked according to their primary drying time. A robust protocol with the shortest primary drying time was considered the optimum and used for experimental verification. Values of the constants used in the optimization exercise are listed in Table 2.

2.10. Process verification

Experimental verification of the protocol predictions was performed. The freezing and the secondary drying protocol as described in section 2.7.3 were complemented with the optimal primary drying protocol. A full shelf was loaded with vials (i.e., 334 units) containing 3.0 ml of the formulation. Process monitoring was performed by equipping eight vials spread across the shelf with a temperature sensor (i.e., 4 × RTD and 4 × TC), these included edge and center positions. Furthermore,

comparative pressure monitoring applying a Pirani and Capacitance pressure sensor was used to evaluate the accuracy of the predictions. Since the product temperature sensors measure the T_b , these data traces were corrected using the predicted ΔT to reflect T_i and make them comparable with the model predictions. At the end of the freeze-drying process, the drying chamber was aerated to atmospheric pressure using nitrogen gas and subsequently the vials were fully stoppered in the freeze-dryer. Ultimately, the vials were capped. These vials were visually inspected for their optical appearance and residual moisture content determined.

2.11. Protocol selection applying the approach proposed by Tang & Pikal

To exemplify the benefits of the presented optimization approach, a classical primary drying protocol, designed by using the approach described by Tang & Pikal (Tang and Pikal, 2004), was simulated. Next, an uncertainty analysis applying the high-resolution variability data was performed on these protocols to evaluate robustness and primary drying time. The approach proposed by Tang & Pikal classifies a formulation based on total solid content and provides basic rules to achieve best guesses of suitable process parameters. Such approach is already an advanced method to derive process parameters compared to commonly used trial-and-error methods. These basic rules were based on extensive process knowledge. At last, the protocol proposed for the ‘low’ T_c formulation by using the Tang & Pikal optimization rules was also verified experimentally in a similar fashion as mentioned in section 2.10.

3. Results and discussion

3.1. Determination of the onset of collapse (T_c) by freeze-drying microscopy

The microscopic images of Fig. 1 were obtained with a freeze-drying microscope. Enlargements of pores and fissures, highlighted using red circles in Fig. 1, indicated onset of collapse of the dried layer. The formulations under study, were either composed of a 10 mg/ml lysozyme solution with 2-hydroxypropyl- β -cyclodextrin (A) as lyoprotectant resulting in an onset of collapse at -12°C or had a lower protein concentration of 1 mg/ml lysozyme with sucrose (B) as lyoprotectant showing the onset of collapse at -33°C . These temperatures were employed as the T_c and should not be exceeded during primary drying to avoid the observed loss of structure.

As expected, usage of 2-hydroxypropyl- β -cyclodextrin as lyoprotectant resulted in a higher T_c as compared to sucrose. This is due to the oligomeric structure of hydroxypropyl- β -cyclodextrin (Serno et al., 2011). Moreover, additionally decreasing the lysozyme concentration in

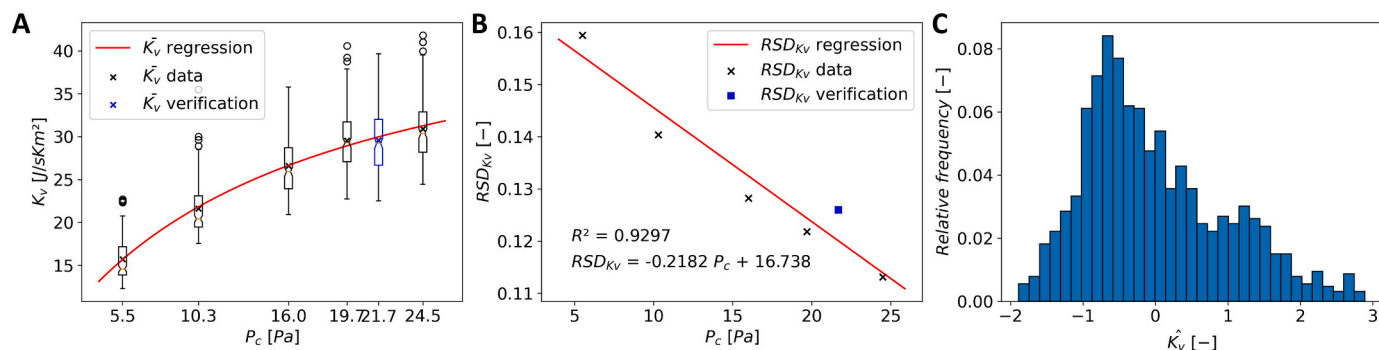


Fig. 2. Graphical representation of the K_v , experimental data and regressions. A: Experimental K_v distribution per pressure level is plotted as a boxplots with empty dots as outliers. The red line represents the weighted non-linear regression of the average. B: RSD_{K_v} at each pressure level is plotted with a marking. The red line represents the linear regression. C: Empirical distribution of normalized K_v data. (For interpretation of the references to colour in this figure legend, the reader is referred to the web version of this article.)

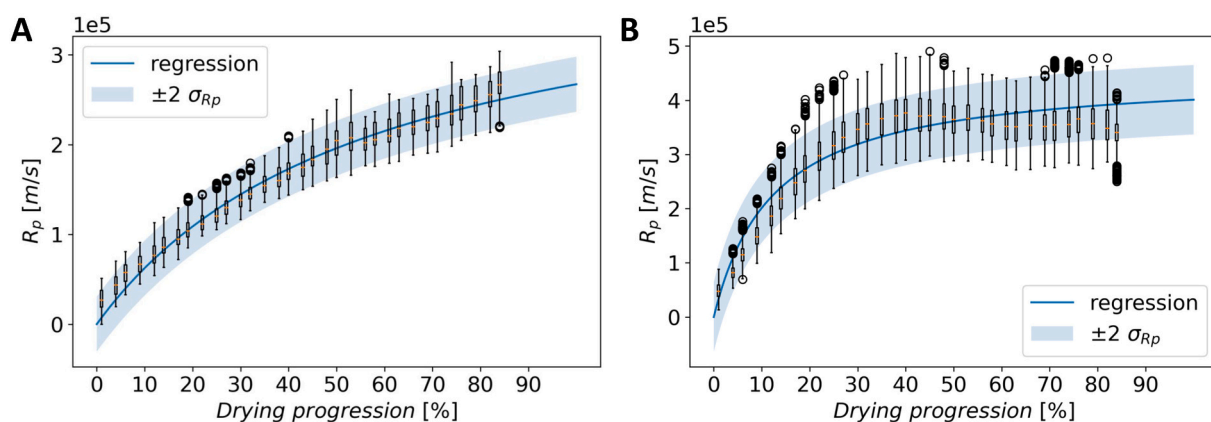


Fig. 3. Graphical representation of the R_p . Experimental data is represented in boxplots with empty dots as outliers, blue line plot represents the R_p regression which is enlarged by $\pm 2 \sigma_{R_p}$ using a blue shaded area. A: 'high' T_c formulation and B: 'low' T_c formulation. (For interpretation of the references to colour in this figure legend, the reader is referred to the web version of this article.)

the 'low' T_c formulation to 1 mg/ml made the formulation more prone to collapse because proteins are known to increase T_c with increasing concentration (Lewis et al., 2010). Two rather different process optimization cases for potential biologics formulations were thus designed in this work. One showing either a high T_c allowing for more aggressive, and a lower T_c requiring more conservative primary drying conditions to avoid failures such as collapse.

3.2. Variability terms for container

Variability terms related to the dimensions of the container such as d_o , d_i and L_t were determined experimentally. The normality of the measured d_o and L_t distributions were confirmed by a comparison of the normally distributed, expected and observed histograms showing reasonable similarity. Therefore, the average and standard deviation of the dataset were sufficient to describe these distributions. For the 6R vials an outer diameter d_o of 10.97 mm with σ_{d_o} of 0.02 mm was measured and an inner diameter d_i of 9.97 mm with σ_{d_i} of 0.03 mm was estimated. Measuring the frozen plug height resulted in an L_t of 12.48 mm and 13.39 mm and a σ_{L_t} of 0.36 mm and 0.35 mm for the 'high' and 'low' T_c formulation, respectively.

A difference of 7% in frozen product layer height (L_t) was observed between both formulations despite applying the same liquid fill volume (i.e., 3.0 ml) and container (i.e., 6R vial). These differences come from the varying total solid content in the two formulations and differences in the contact angle of the formulations with the glass container. Experimental measurements confirmed this since a contact angle of $65.2^\circ \pm 4.3^\circ$ for the 'low' T_c and $47.7^\circ \pm 2.0^\circ$ for the 'high' T_c formulations with the glass vial was determined. The excipient 2-hydroxypropyl- β -cyclodextrin is known to have surfactant-like behavior thus lowering the contact angle (Zhang et al., 2022).

3.3. Variability terms for heat transfer

The K_v was determined using the gravimetric method on individual vials leading to a high-resolution data set. Fig. 2 depicts the experimental data and the regressions that describe the variability terms of K_v . The dependency of the K_v on P_c could be described by using $\alpha = 3.86$, $\beta = 2.93$ and $\gamma = 0.066$ by applying Eq. (8) with an RMSE of 0.34 J/(sK 2). A good correlation ($R^2 = 0.930$) between RSD_{K_v} and P_c was found, with higher pressures leading to a smaller relative variation in K_v . This relationship was approximated by a linear regression according to Eq. (9) with $a_{K_v} = -0.2182$ and $b_{K_v} = 16.738$. As reflected by the histogram of normalized values, K_v does not follow the typical bell curve of a normal distribution. The bi-modal distribution has a main population just below the average and a smaller tailing peak towards higher values.

Since it is complex to mathematically describe non-normal multimodal distributions, it was opted for randomly resampling from this empirical distribution. At last, the independent verification experiment at P_c of 22 Pa with alternate T_s fits well within the K_v and RSD_{K_v} regressions as indicated by the blue markers in Fig. 2A, B, which confirms the independence of these regressions towards T_s .

A novel part of this study was the methodology to describe the distribution of the K_v parameter. Previous modelling work either assumed a normal distribution, or at best split the K_v in an edge and center population with distinct values (Mortier et al., 2016; Fissore and Pisano, 2015; Koganti et al., 2011; Juckers et al., 2022). The current work exemplifies that the K_v is not distributed normally across the shelf (see Fig. 2). To the contrary, a multimodal distribution can be observed which resembles the traditional corner, edge and center vial classifications, but with a full continuum in between these populations. Applying an empirical distribution of normalized K_v values within the modelling framework was able to better represent the reality and enabled a prediction of the primary drying end across a full batch.

During the characterization of K_v , the typical interdependencies between process parameters were observed. For example, the measured K_v depended on the applied P_c as more gas molecules lead to a better heat transfer by gas-conduction (Pikal et al., 2016). Additionally, a higher number of directly contacting neighbor vials lowers the K_v , which is important for the corner and edge vials. This is rather due to the endothermic cooling effect by sublimation in the whole configuration than to heat radiation from uncooled surfaces (Ehlers et al., 2021). In addition, the high-resolution data of K_v showed that the relative variability across the shelf dropped when applying a higher P_c . Variation in K_v across the shelf is mainly driven by inter-vial differences in heat radiation (Rambhatla and Michael, 2003) and cooling due to heat conduction from neighboring vials (Ehlers et al., 2021). Upon increasing P_c , the more homogenous gas-conduction mechanism will play a bigger role explaining the lower RSD_{K_v} .

3.4. Variability terms for dried product layer resistance

It was opted to characterize the R_p based on product temperature data and not Tunable Diode Laser Absorption Spectroscopy (TDLAS) or Manometric Temperature Measurement (MTM) for a couple of reasons. At first, we are interested in the intra-batch variation of R_p as an input for the uncertainty analysis, which TDLAS or MTM cannot deliver since they only yield a batch average R_p profile. Secondly, during an MTM measurement the T_i will briefly rise. Since we are interested in verifying primary drying protocols that are close to but not exceed the T_c , MTM as product temperature technique could potentially induce collapse. At last, with the applied freeze-dryer it was technically not feasible to perform TDLAS or

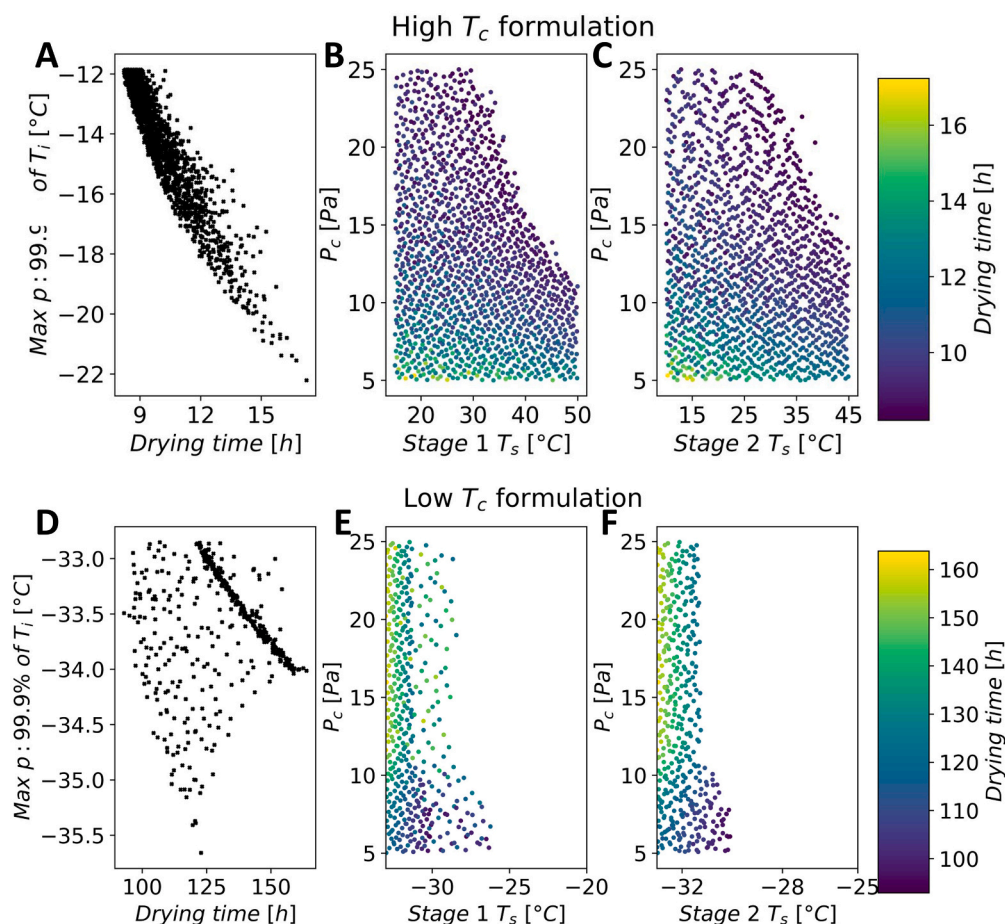


Fig. 4. Graphical overview of the optimization exercise of the ‘high’ (A, B, C) and ‘low’ (D, E, F) T_c formulation. A/D: Scatter plot of both outcomes of the uncertainty analysis from all robust protocols. B/E: Scatter plot where dots are colored according drying time originating from protocols defined by optimization factor Stage 1 T_s versus P_c . C/F: Scatter plot where dots are colored according primary drying time originating from protocols defined by optimization factor Stage 2 T_s versus P_c .

MTM accurately due the absence of a duct or fast-moving valve between condenser and drying chamber.

The R_p and its variability terms were determined independently for each formulation (Fig. 3). The relationship between R_p^- and L_d could be described using Eq. (12) with $R_{p0} = 20,735$; $A = 4.33 \cdot 10^7$ and $B = 89.6$ for the ‘high’ T_c formulation and in case of the ‘low’ T_c formulation with $R_{p0} = 0$; $A = 2.72 \cdot 10^8$ and $B = 603$. Upon pooling the standard deviation across all bins an σ_{R_p} of 15,353 and 32,067 was obtained for the ‘high’ or ‘low’ T_c formulation, respectively.

As evidenced by Fig. 3, R_p increases as primary drying progresses. This behavior is typical during freeze-drying because the path length that vapor molecules must travel under Knudsen flow conditions enlarges as sublimation continues (Pikal et al., 1984). This R_p increase is formulation dependent since all formulation components influence the ice crystal formation during freezing and thus pore morphology of the dried product layer (Lu and Pikal, 2004). The ‘low’ T_c formulation displayed higher R_p values in comparison with the ‘high’ T_c formulation, because of the higher solid content, which will result in a lower dried layer porosity.

3.5. Process optimization

In the next step, the effect of the optimization factors listed in Table 1 on the model outcomes of the uncertainty analysis: $\max p: 99.9\% T_i$ and primary drying time was evaluated. Protocols with a lower $\max p: 99.9\% T_i$ are associated with a lower RoF since the safety margin towards T_c is larger. All the assessed protocols that led to a robust process prediction

Table 3

Factors describing the optimal primary drying protocol obtained from the process optimization strategy.

Optimization factor	‘High’ T_c Formulation	‘Low’ T_c Formulation
Stage 1 T_s [°C]	41	-26
Stage 1 hold time [h]	0.82	1.50
T_s ramp [°C/h]	8.75	0.39
Stage 2 T_s [°C]	30	-30
P_c [Pa]	20	5

(i.e., $\max p: 99.9\% T_i < T_c$) are represented by a single dot in the scatter plots of Fig. 4. Out of the 4096 protocols screened in this optimization exercise, 1413 for the ‘high’ T_c formulation and 427 for the ‘low’ T_c formulation proved to be robust. The least risky protocols, dots in Fig. 4A, D with a lower $\max p: 99.9\% T_i$, generally come with a longer drying time.

Plots of the stage 1 and stage 2 T_s against the P_c of robust protocols show the dependency of these factors on the drying time (Fig. 4B, C, E, F). For the ‘high’ T_c formulation, a different chamber pressure range was necessary to achieve the shortest primary drying times as compared to the ‘low’ T_c formulation. Moreover, no robust protocols were obtained when combining a high T_s with a high P_c . Ultimately, the two-stage protocol approach was affirmed as higher stage 1 T_s than stage 2 T_s values were feasible. No straightforward dependency of the optimization factors stage 1 hold time and T_s ramp on any model outcome could be observed. The combinations of factors describing the optimal primary

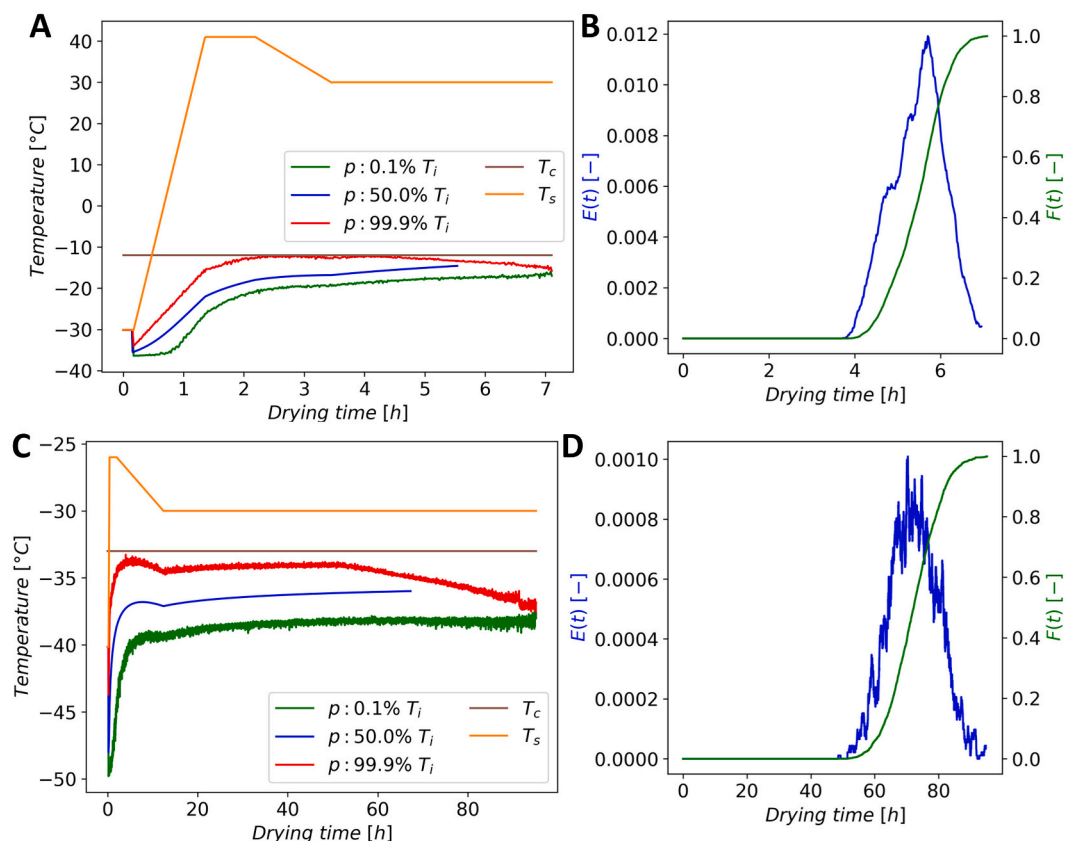


Fig. 5. Graphical overview of the most optimal scenario for the 'high' (A, B) and 'low' (C, D) T_c formulation. A/C: Temperature plot with the two-stage T_s protocol (orange), T_c (brown), and the 0.1 (green), 50.0 (blue) and 99.9 (red) percentile values of the T_i distribution. B/D: Relative distribution of end of primary drying in blue and its cumulative curve in green. (For interpretation of the references to colour in this figure legend, the reader is referred to the web version of this article.)

drying protocols are listed in Table 3.

The in-silico predictions including the results of the uncertainty analysis are shown in Fig. 5A and C, which represents the predicted temperature plot for each formulation. The optimization exercise was able to identify protocols where $p: 99.9\%$ T_i was maximized but where it was kept below T_c . The model predicted lower risks of failure towards the final phase of primary drying, demonstrated by the decline of the $p: 99.9\%$ T_i trace. This decline starts when the first samples are predicted to be free of ice (see Fig. 5B, D). Since the vials with higher K_v complete their primary drying phase earlier, they are excluded earlier from the uncertainty analysis. Near the end of the primary drying phase the dataset only comprises samples with reduced risk.

For the 'high' T_c formulation, the first vials were predicted to complete primary drying after 3.7 h, and 99.9% of the vials after 7.1 h of the primary drying protocol (Fig. 4B). Instead, for the 'low' T_c formulation the first vial should finish primary drying after 50.3 h, and the whole protocol should take 93.5 h to allow completion of primary drying for 99.9% of the batch (Fig. 4D).

The two-phase protocol approach took advantage of the lower R_p values at the start of primary drying. By keeping the 99.9th percentile of T_i as close as possible to T_c during the entire duration of primary drying, the sublimation rate was maximized, and the primary drying time minimized without causing collapse. The space for optimization by applying a two-phase T_s greatly depends on the shape of the R_p profile. In the 'low' T_c formulation, the R_p profile flattens out rather early. This resulted in a relatively shorter period during which the higher stage 1 T_s could be applied. It must be noted that the optimized primary drying protocol is only valid in these specific conditions, as the R_p profile is specific to a certain formulation and freezing protocol (Kasper and Friess, 2011).

Whereas for the 'high' T_c formulation drying at a P_c of 20 Pa was identified as fastest, a P_c of 5 Pa was optimal for the 'low' T_c formulation.

Overall, a higher P_c is preferred under aggressive freeze-drying conditions as used in case of the 'high' T_c formulation. This might seem counterintuitive as a lower P_c would increase the pressure differential that drives sublimation. However, as mentioned earlier and shown in Fig. 2, a lower P_c will increase the intra-batch variability of K_v . It seems that an overall reduction of the intra-batch variability is opportune in aggressive freeze-drying conditions, as it leads to a shorter drying time of the slowest drying vials. Choosing the optimal P_c is a tradeoff between maximizing the driving force of sublimation versus intra-batch variability. In contrast, for the conservative freeze-drying case as needed for our 'low' T_c formulation this tradeoff was shifted towards the lower P_c levels. This fine balance exemplifies the need of mechanistic models that include variability terms to find the most suitable P_c .

3.6. Process verification

The optimal protocols derived from modelling were experimentally verified. Fig. 6 shows the T_i derived from the product temperature sensors and the prediction interval $p: 0.1-99.9\%$ T_i . Both compact PT100 (i.e., RTD1-4) and thermocouples (i.e., TC1-4) were used as product temperature sensors. For both formulations the measured T_i traces from TC were all within the prediction interval and did not exceed the T_c limit. After loss of contact with the frozen product, these traces showed the end of primary drying with the typical deviation towards higher temperatures.

In general, the TC sensors tend to show a later onset of the end of primary drying than the RTD sensors (Fig. 6). This observation was confounded with variations in K_v as both sensors were spread across the shelf including edge and center positions. Furthermore, the transition phase at the end of primary drying was shorter for the TC sensors compared to the RTD sensors. Both observations can be explained by the

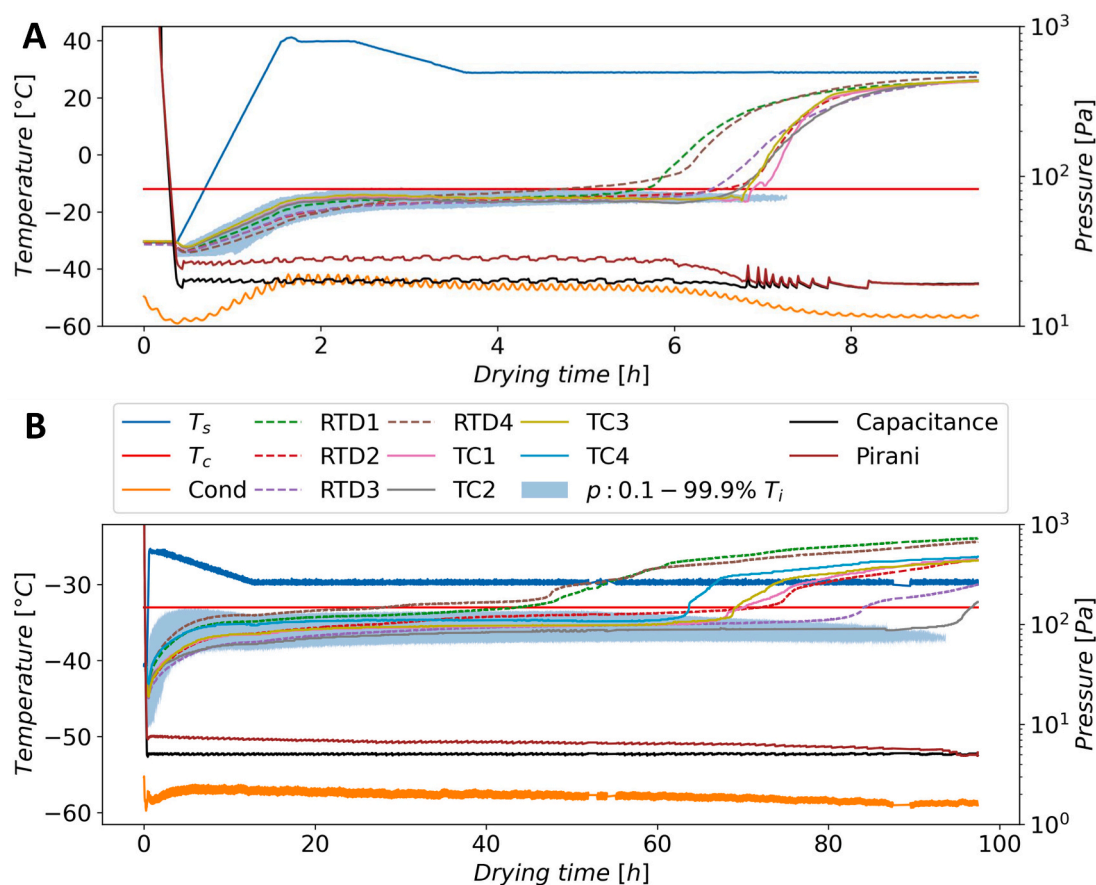


Fig. 6. Graphical overview of the verification experiments with process data overlaid with the predictions (blue area) for the ‘high’ (A) and the ‘low’ (B) T_c formulation. Cond represents the condenser temperature. (For interpretation of the references to colour in this figure legend, the reader is referred to the web version of this article.)

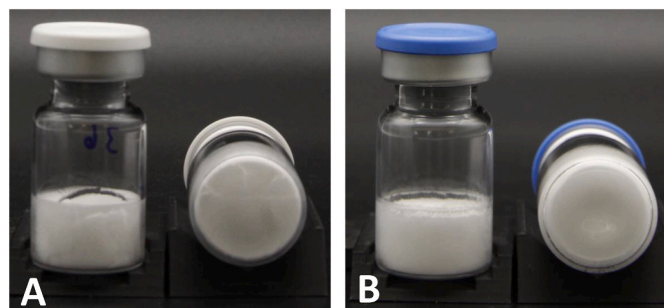


Fig. 7. Vial appearance of ‘high’ (A) and ‘low’ (B) T_c formulation of the verification experiment.

fact that TC sensors yield a point measurement, whereas the compact RTD sensors reflect the average temperature across the probe head. TC sensors are therefore recommended as they yield more precise product temperature measurements (Nail et al., 2017).

In the case of the ‘high’ T_c formulation, the onset of deviation of the product temperature traces started at around 4.7 h and ended at around 7.0 h. In contrast, for the ‘low’ T_c formulation this first onset of deviation was after 49 h and the last onset after 88 h. The timing of these onsets corresponds well with the distribution of drying time (Fig. 5B, D). Furthermore, comparative pressure measurement indicated the end of primary drying close to the predicted drying time for both the ‘high’ and the ‘low’ T_c formulation.

The residual moisture content after secondary drying was affected by the formulation composition. It was overall low with $0.35 \pm 0.05\%$ and

Table 4

Summary of the primary drying protocol using the approach proposed by Tang & Pikal and outcomes of uncertainty analysis of these protocols.

Parameter	‘High’ T_c Formulation	‘Low’ T_c Formulation
Target T_i [°C]	-17	-35
T_s [°C]	20	-28
P_c [Pa]	18.4	8.4
Primary drying time [h]	9.09	80.5
Max p: 50.0% T_i [°C]	-19.1	-33.4
Max p: 99.9% T_i [°C]	-14.4	-31.6

$1.70 \pm 0.29\%$ for the ‘high’ and ‘low’ T_c formulation, respectively. This final residual moisture content is dependent on the secondary drying protocol which we held consistent for 6 h at 25 °C. Each protein has an optimal residual moisture content to promote storage stability, which should be targeted by adapting the secondary drying protocol (Hsu et al., 1992).

At last, the lyophilized cakes were of elegant appearance without signs of collapse (Fig. 7). Minor shrinkage and appearance of small cracks were attributed to the fully amorphous nature of the cakes and not considered to be evidence of collapse (Ullrich et al., 2015). All experimental outcomes of the verification experiments indicated that the predicted optimized protocols were robust.

3.7. Protocol selection applying the approach proposed by Tang & Pikal

As a benchmark, we applied the approach proposed by Tang & Pikal (Tang and Pikal, 2004) to predict primary drying protocols for the ‘low’ and ‘high’ T_c formulation. The optimization rules defined by Tang &

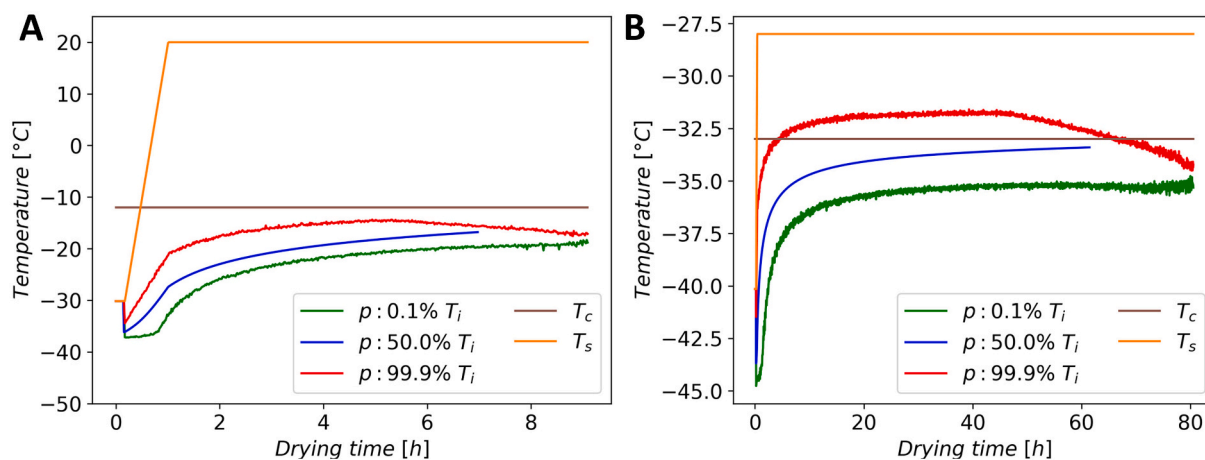


Fig. 8. Process predictions based on the primary drying protocol recommendation of Tang & Pikal (Tang and Pikal, 2004) for the ‘high’ (A) and ‘low’ (B) T_c formulations.

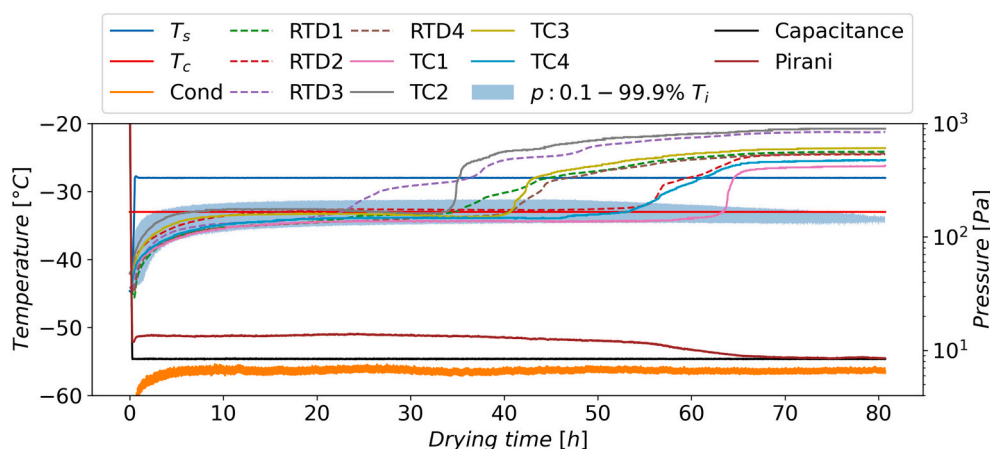


Fig. 9. Graphical overview of the verification experiment for ‘low’ T_c formulation based on the primary drying protocol recommendation of Tang & Pikal (Tang and Pikal, 2004). Process data is overlaid with the predictions (blue area). Cond represents the condenser temperature. (For interpretation of the references to colour in this figure legend, the reader is referred to the web version of this article.)

Pikal led to the primary drying protocols summarized in Table 4, and displayed in Fig. 8 for both formulations.

For the ‘high’ T_c formulation, a safety margin of 5 °C was prescribed leading to a target T_i of -17 °C. The obtained T_s of 20 °C and the P_c of 18.4 Pa reflect a more conservative drying process compared to the process resulting from the optimization (section 3.5). The median T_i was estimated to be maximally 2.1 °C lower than the targeted value. Moreover, the $max p$: 99.9% T_i was located at -14.4 °C. This indicates a robust process at the expense of a drying time of 9.1 h which is 28% longer than the protocol resulting from our optimization approach. Our optimized aggressive approach resulted in sufficiently dried product

with an acceptable cake appearance. Therefore, we refrained from experimentally verifying the more conservative primary drying setting proposed by Tang & Pikal, because these will evidently lead to longer process times without inducing collapse.

For the ‘low’ T_c formulation (Fig. 8B), the protocol obtained by the approach proposed by Tang & Pikal rendered a substantially higher risk profile than the proposed RoF of 0.1%. The estimated median T_i of up to -33.4 °C was just below T_c but the $max p$: 99.9% T_i was situated at -31.6 °C, meaning that a substantial part of the batch would experience conditions that lead to signs of collapse. In addition, the primary drying time according to the approach proposed by Tang & Pikal was estimated



Fig. 10. Vial appearances from the verification experiment for ‘low’ T_c formulation based on the primary drying protocol recommendation of Tang & Pikal (Tang and Pikal, 2004).

to be 80.5 h, which is 13 h shorter than the protocol obtained from our optimization approach. However, the Tang & Pikal protocol would not be deemed robust according to the uncertainty as the risks far exceed the proposed RoF.

The 'low' T_c formulation was experimentally verified applying the protocol defined by the Tang & Pikal optimization rules. The process data is shown in Fig. 9. The measured T_i traces were within the prediction interval and did exceed the T_c limit as anticipated by the model. However, the onset of the deviation of the T_i traces near end of primary drying and comparative pressure measurement indicated a shorter primary drying time than the model predictions. Since a substantial number of samples had their T_i near or above the T_c limit of -32 °C, micro-structural changes are expected to occur in these samples. It is known that these micro-structural changes can decrease the R_p thus shortening the process (Fissore and Pisano, 2015). Since the mechanistic model does not take these R_p shifts into account, protocol predictions that results in samples above the T_c limit are therefore not fully accurate.

The lyophilized product of the 'low' T_c formulation dried with the primary drying protocol based on the approach proposed by Tang & Pikal displayed micro-structural changes, evidenced by the cake appearances displayed in Fig. 10. About 32% of the samples did not show external signs of (micro)-collapse thus displaying an elegant appearance (Fig. 10A). Next, 37% of the batch showed minimal evidence of micro-structural (Fig. 10B) because a single dent was observed, and 31% of the batch showed multiple dents near the bottom of the sample (Fig. 10C). The residual moisture content of the samples was characterized at $1.79 \pm 0.45\%$. The higher relative standard deviation (RSD) in residual moisture content of this batch in comparison with the one obtained from the optimized protocol (i.e., RSD: 25% versus 17%) is likely the result of observed partial (micro)-collapse.

4. Conclusions

In this work a model-based process development methodology that can result in fast and at the same time robust primary drying protocols was developed and experimentally verified. An in-silico optimization strategy applying a two-stage shelf temperature protocol was employed to reduce the drying time. This was combined with an uncertainty analysis to estimate the risks associated with the proposed primary drying protocols. To this end, two rather different process optimization cases for potential biologics formulations were selected, showing either a high T_c allowing for more aggressive, and a lower T_c requiring more conservative primary drying conditions.

The heat-mass models worked well as evidenced by the verification experiments. Both the experimental drying times and the T_i traces were in very good agreement with the predictions of the optimal protocols. Moreover, an acceptable residual moisture content and no signs of cake collapse were observed.

Furthermore, our data-driven methodology could propose more economical primary drying protocols than these obtained by the Tang & Pikal optimization rules, which per se is already smart and based on an enormous experience. When aggressive freeze-drying conditions were applied, the optimization approach utilizing an uncertainty analysis could provide a substantially faster protocol. In case of the conservative freeze-drying conditions, the proposed approach led to a protocol with less samples at risk of collapse and consequently less vial rejections. A data-driven decision of the process parameters is therefore more applicable for a Quality-by-Design strategy compared to an experience-driven decision as described by Tang & Pikal.

The effort of performing the detailed experiments to obtain the high-resolution variability data and the execution of in-silico optimization proved to be a highly suitable approach to achieve a fast and yet robust freeze-drying cycle.

CRedit authorship contribution statement

Brecht Vanbillemont: Conceptualization, Data curation, Formal analysis, Investigation, Project administration, Methodology, Software, Validation, Writing – original draft, Writing – review & editing. **Anna-Lena Greiner:** Data curation. **Vanessa Ehrh:** Data curation. **Tim Menzen:** Writing – review & editing. **Wolfgang Friess:** Conceptualization, Resources, Supervision, Writing – review & editing. **Andrea Hawe:** Conceptualization, Resources, Project administration, Supervision, Writing – review & editing.

Declaration of Competing Interest

The authors declare that they have no known competing financial interests.

Data availability

Data will be made available on request.

References

- Carfagna, Marco, et al., 2020. Heat flux sensor to create a design space for freeze-drying development. *Eur. J. Pharm. Biopharm.* 153, 84–94.
- Carpenter, John F., Pikal, Michael J., Chang, Byeong S., Randolph, Theodore W., 1997. Rational design of stable lyophilized protein formulations: some practical advice. *Pharm. Res.* 14, 969–975.
- De Meyer, Laurens, et al., 2017. Modelling the primary drying step for the determination of the optimal dynamic heating pad temperature in a continuous pharmaceutical freeze-drying process for unit doses. *Int. J. Pharm.* 532 (1), 185–193.
- Ehlers, Sarah, Schroeder, Rudolf, Friess, Wolfgang, 2021. Trouble with the Neighbor during Freeze-Drying: Rivalry about Energy. *J. Pharm. Sci.* 110 (3), 1219–1226.
- Fissore, Davide, Pisano, Roberto, 2015. Computer-aided framework for the design of freeze-drying cycles: optimization of the operating conditions of the primary drying stage. *Processes* 3 (2), 406–421.
- Gamiz, Ana Gabriela Renteria, et al., 2019. Freeze drying in the biopharmaceutical industry: an environmental sustainability assessment. *Food Bioprod. Process.* 117, 213–223.
- Hsu, C.C., et al., 1992. Determining the optimum residual moisture in lyophilized protein pharmaceuticals. *Dev. Biol. Stand.* 74, 255–270.
- Juckers, Alex, et al., 2022. Model-based Product Temperature and Endpoint Determination in primary Drying of Lyophilization Processes. *Pharmaceutics* 14 (4), 809.
- Kasper, Julia Christina, Friess, Wolfgang, 2011. The freezing step in lyophilization: Physico-chemical fundamentals, freezing methods and consequences on process performance and quality attributes of biopharmaceuticals. *Eur. J. Pharm. Biopharm.* 78 (2), 248–263.
- Koganti, Venkat Rao, et al., 2011. Investigation of design space for freeze-drying: use of modeling for primary drying segment of a freeze-drying cycle. *AAPS PharmSciTech* 12 (3), 854–861.
- Lewis, Lavinia M., et al., 2010. Characterizing the freeze-drying behavior of model protein formulations. *AAPS PharmSciTech* 11 (4), 1580–1590.
- Leys, Laurens, et al., 2020. A primary drying model-based comparison of conventional batch freeze-drying to continuous spin-freeze-drying for unit doses. *Eur. J. Pharm. Biopharm.* 157, 97–107.
- Lu, Xiaofeng, Pikal, Michael J., 2004. Freeze-drying of mannitol-trehalose-sodium chloride-based formulations: the impact of annealing on dry layer resistance to mass transfer and cake structure. *Pharm. Dev. Technol.* 9 (1), 85–95.
- Mortier, Séverine Thérèse F.C., et al., 2016. Uncertainty analysis as essential step in the establishment of the dynamic Design Space of primary drying during freeze-drying. *Eur. J. Pharm. Biopharm.* 103, 71–83.
- Murphy, Daniel M., Koop, Thomas, 2005. Review of the vapour pressures of ice and supercooled water for atmospheric applications. *Quarter. J. Royal Meteorol. Soc.: J. Atmos. Sci., Appl. Meteorol. Phys. Oceanogr.* 131 (608), 1539–1565.
- Nail, Steven L., et al., 2002. Fundamentals of freeze-drying. *Develop. Manuf. Protein Pharmaceut.* 281–360.
- Nail, Steven, et al., 2017. Recommended best practices for process monitoring instrumentation in pharmaceutical freeze drying—2017. *AAPS PharmSciTech* 18 (7), 2379–2393.
- Patel, Sajal Manubhai, Pikal, Michael J., 2013. Lyophilization process design space. *J. Pharm. Sci.* 102 (11), 3883–3887.
- Patel, Sajal M., Chaudhuri, Swetaprovo, Pikal, Michael J., 2010. Choked flow and importance of Mach I in freeze-drying process design. *Chem. Eng. Sci.* 65 (21), 5716–5727.
- Pikal, M.J., Roy, M.L., Shah, Saroj, 1984. Mass and heat transfer in vial freeze-drying of pharmaceuticals: Role of the vial. *J. Pharm. Sci.* 73 (9), 1224–1237.
- Pikal, Michael J., et al., 2016. Freeze-drying process development and scale-up: scale-up of edge vial versus center vial heat transfer coefficients, *Kv. J. Pharm. Sci.* 105 (11), 3333–3343.

- Pisano, Roberto, Fissore, Davide, Barresi, Antonello A., 2011. Heat transfer in freeze-drying apparatus. *Develop. Heat Transf.* 10, 23799.
- Rambhatla, Shailaja, Michael, J. Pikal, 2003. Heat and mass transfer scale-up issues during freeze-drying, I: atypical radiation and the edge vial effect. *Aaps PharmSciTech* 4, 22–31.
- Rasetto, Valeria, et al., 2010. On the use of a dual-scale model to improve understanding of a pharmaceutical freeze-drying process. *J. Pharm. Sci.* 99 (10), 4337–4350.
- Rhieu, Steve Y., Anderson, David D., Janoria, Kumar, 2020. A Regulatory Perspective on Manufacturing Processes Pertaining to Lyophilized Injectable Products. *AAPS J.* 22 (5), 1–8.
- Scutella, Bernadette, et al., 2018. Determination of the dried product resistance variability and its influence on the product temperature in pharmaceutical freeze-drying. *Eur. J. Pharm. Biopharm.* 128, 379–388.
- Serno, Tim, Geidobler, Raimund, Winter, Gerhard, 2011. Protein stabilization by cyclodextrins in the liquid and dried state. *Adv. Drug Deliv. Rev.* 63 (13), 1086–1106.
- Sobol, I.M., 1967. On the distribution of points in a cube and the approximate evaluation of integrals. *USSR Comput. Math. Math. Phys.* 7, 86–112.
- Strongrich, Andrew, Alexeenko, Alina, 2021. Wireless sensor networks for pharmaceutical lyophilization: Quantification of local gas pressure and temperature in primary drying. *Eur. J. Pharm. Biopharm.* 169, 52–63.
- Tang, Xiaolin Charlie, Pikal, Michael J., 2004. Design of freeze-drying processes for pharmaceuticals: practical advice. *Pharm. Res.* 21 (2), 191–200.
- Tang, Xiaolin Charlie, Nail, Steven L., Pikal, Michael J., 2006. Evaluation of manometric temperature measurement, a process analytical technology tool for freeze-drying: part II measurement of dry-layer resistance. *AAPS PharmSciTech* 7 (4), E77–E84.
- Tchessalov, Serguei, et al., 2022. Best Practices and guidelines (2022) for Scale-up and Tech transfer in Freeze-Drying based on Case Studies. Part I: challenges during Scale up and transfer. *AAPS PharmSciTech* 24 (1), 11.
- Ullrich, Sabine, Seyferth, Stefan, Lee, Geoffrey, 2015. Measurement of shrinkage and cracking in lyophilized amorphous cakes. Part I: final-product assessment. *J. Pharm. Sci.* 104 (1), 155–164.
- Vanbillemont, Brecht, De Beer, Thomas, 2020. Model-based optimization of the primary drying phase of oral lyophilizates. *Int. J. Pharm.* X 2, 100057.
- Vanbillemont, Brecht, Nicolai, Niels, Leys, Laurens, De Beer, Thomas, 2020. Model-based optimisation and control strategy for the primary drying phase of a lyophilisation process. *Pharmaceutics* 12 (2), 181.
- Velardi, Salvatore A., Barresi, Antonello A., 2008. Development of simplified models for the freeze-drying process and investigation of the optimal operating conditions. *Chem. Eng. Res. Des.* 86 (1), 9–22.
- Zhang, Hailong, et al., 2022. Polysorbates versus Hydroxypropyl Beta-Cyclodextrin (HPβCD): Comparative Study on Excipient Stability and Stabilization Benefits on Monoclonal Antibodies. *Molecules* 27 (19), 6497.